Coherent and incoherent damping pathways mediated by strong coupling of two-dimensional atomic crystals with metallic nanogrooves

Song Zhang,[1] Hong Zhang,[1] Ting Xu,[2] Wenxin Wang,[3] Yuhang Zhu,[1] Daimin Li,[1] Zhiyi Zhang,[1] Juemin Yi,[4] and Wei Wang[1,*]

[1]*College of Physical Science and Technology, Sichuan University, 610064, Chengdu, China*

[2]*National Laboratory of Solid State Microstructures, College of Engineering and Applied Sciences and Collaborative Innovation Center of Advanced Microstructures, Nanjing University, 210093, Nanjing, China*

[3]*Institut für Physik & IMN MacroNano® (ZIK) Technische Universität Ilmenau, 98693, Ilmenau, Germany*

[4]*Institut für Physik, Carl von Ossietzky Universität, D-26111, Oldenburg, Germany*

(Received 17 April 2018; revised manuscript received 10 May 2018; published 1 June 2018)

In this paper we investigate the strong exciton-plasmon coupling in a hybrid system consisting of an atomic thick WS_2 monolayer and a gold nanogroove array. We theoretically identify the coexistence of two damping pathways: a coherent damping pathway resulting from the resonant dipole-dipole interaction and a coupling-induced incoherent damping pathway due to the spontaneous emissions of a photon by one subsystem and its subsequent reabsorption by the other. We show that the interplay between both interaction processes not only determines the optical property of the hybrid system, but also results in a pronounced modification of the radiative damping due to the formation of super- and subradiant polariton states. Importantly, we reveal that the radiative damping property of the polariton modes is determined only by the effect of coupling-induced sub- and super-radiance, which is distinctly different from that previously observed in a metal-molecular hybrid system where pure dephasing of J-aggregate excitons dominates the polariton dynamics. Our findings may pave the way towards active manipulation of polariton dynamics and offer possibilities for realizing coherent active control in novel plasmonic devices.

DOI: 10.1103/PhysRevB.97.235401

I. INTRODUCTION

Strong light-matter coupling manifested by Rabi splitting has attracted tremendous attention due to its fundamental importance in cavity quantum-electrodynamics research and great potentials in quantum information applications [1,2]. Strong coupling occurs when the coupling strength between the two individual systems exceeds the damping of either [3–8]. A large variety of strong coupling phenomena are observed in the case of light-matter interaction, in particular, strong coupling between fundamentally distinct emitters [9]: excitons (Xs) in organic/inorganic semiconductors or J-aggregated molecules and surface plasmon polaritons (SPPs) supported by plasmonic nanostructures has been extensively studied [10–18]. SPPs are optical excitations at the metal-dielectric interface, which can tightly confine light on the nanoscale [19–21], leading to a strongly enhanced local field with ultrasmall mode volume and hence enabling strong X-SPP coupling with giant Rabi splitting of up to several hundred meV [10,11,22–25].

Importantly, our previous work has shown that, in these X-SPP hybrid systems, the individual system not only couples to each other via coherent dipole-dipole interactions, but also radiatively couples to the environment via incoherent exchange of photon energy [17]. The interplay between coherent and incoherent interaction processes plays an important role in determining the energetics of the system. It also governs the corresponding dynamics by altering the radiative damping of the hybrid modes, leading to cooperative emission phenomena known as sub- and super-radiance [26]. These sub- and super-radiant effects have also been observed in many other strongly coupled systems such as trapped ions [27], molecular aggregates [28], excitonic quantum dots [29] and wells [30], and plasmonic excitations in nanostructures [9,31–34].

Recently, two-dimensional (2D) transition metal dichalcogenides (TMDs), a new emerging class of atomic crystals, have attracted intense interest as a prototype system for studying strong light-matter coupling. As the bulk crystal transitions to the 2D limit (monolayer), TMDs evolve from an indirect band gap semiconductor to one with a direct band gap at the K (K') points of the Brillouin zone, leading to large binding energies due to the reduced dielectric screening and the quantum confinement of excitons [35]. This makes them excellent candidates for achieving strong light-matter interactions. As crystalline semiconductors, they have significantly less inhomogeneous broadening with high photostability compared to traditional semiconductors such as molecular aggregates. Moreover, atomically thin TMDs are more integratable than organic molecules in practical applications for ultrathin and flexible plasmonic devices.

Recent studies have demonstrated strong coupling in monolayer TMDs with various plasmonic nanostructures or nanocavities including gold nanoparticle [36], hole array [37], nanorod [38,39], silver nanodisk lattice [40], and DBR microcavity [41–43]. Rabi splitting energy over 100 meV has been reported. In contrast to the great progresses in investigations on the coherent interaction of the strongly coupled TMD-based hybrid systems, the incoherent interaction and thus on the

*w.wang@scu.edu.cn

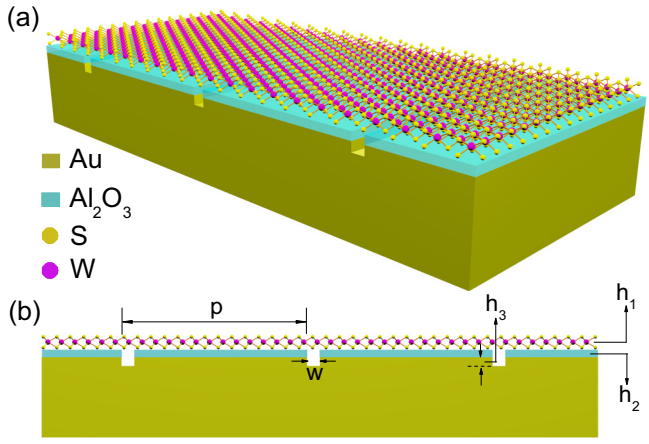

FIG. 1. (a) A three-dimensional schematic of the coupled system with a monolayer WS_2 on a gold nanogroove array. (b) Cross section of the hybrid nanostructure with nanogroove period $p = 430$ nm, groove width $w = 45$ nm, and groove depth $h_3 = 30$ nm. A thin layer of Al_2O_3 separates the monolayer WS_2 from the gold nanogroove array to eliminate the charge transfer. The thickness of monolayer WS_2 and Al_2O_3 layer is $h_1 \approx 1$ nm and $h_2 = 5$ nm, respectively.

interplay between the strong coupling and the radiative damping properties of the hybrid systems still remain unexplored.

In this paper we report on the interplay between strong coupling and radiative damping of strongly coupled 2D atomic crystal and surface plasmons in a hybrid system consisting of an atomic thick tungsten disulfide (WS_2) monolayer and a gold nanogroove array. We theoretically identify the coexistence of two damping pathways: a coherent damping pathway resulting from the resonant dipole-dipole interaction and an incoherent damping pathway due to the spontaneous emissions of a photon by one emitter and its subsequent reabsorption by another. By using full wave simulations and introducing a coupling-induced cross-damping term in our coupled oscillator model, we show that the interplay between both pathways results in a pronounced modification of the radiative damping due to the formation of super- and subradiant polariton states. We expect that a strong modification on the radiative damping can pave the way towards realizing coherent active control in novel plasmonic devices.

II. RESULTS AND DISCUSSION

A. Optical property of a strongly coupled system

The hybrid nanostructure investigated here consists of a monolayer WS_2 covered on top of a gold nanogroove array, as depicted in Fig. 1(a). A thin layer of Al_2O_3 with thickness of $h_2 = 5$ nm is introduced to eliminate the charge transfer between monolayer WS_2 and a gold nanogroove array. A cross section view of the hybrid system is given in Fig. 1(b). The 2D WS_2 monolayer possess the advantage that it exhibits up to ~20% isolated room-temperature optical absorption at A exciton resonance around 2 eV due to strong exciton oscillator strength, making it a favorable choice for light-matter strong coupling. The nanogroove array with shallow depth and small groove width is chosen to minimize radiative damping, thus providing spectrally narrow SPP resonances with correspondingly long lifetimes [31,44].

To investigate the strong X-SPP coupling in the hybrid system, we first performed full wave simulations to obtain its optical response by using the commercial finite element (FEM) solver COMSOL Multiphysics. For the modeling of the optical response of the WS_2 monolayer, its dielectric function as a function of photon energy E (in unit of eV) is described by the superposition of several Lorentzian oscillators [37,45,46]:

$$\varepsilon(E) = \varepsilon_B + \sum_{j=1}^{N} \frac{f_j}{E_{0j}^2 - E^2 - iE\Gamma_j}. \quad (1)$$

Here f_j, E_{0j}, and Γ_j are, respectively, oscillator strength, resonance energy, and damping rate of the oscillator with index j. ε_B representing the background dielectric contribution can be assumed as unity because of the monolayer structure of WS_2. These parameters applied in our simulation are from the data in Ref. [37], where the measured optical spectra of a monolayer WS_2 flake on quartz have been very nicely reproduced by using Eq. (1). Note that in our simulation we use the measured spectral width of the A exciton resonance $\hbar\Gamma_X = 28$ meV, which is dominated by the radiative and nonradiative damping processes, providing a homogeneously broadened absorption spectrum [37]. We will show later in detail that the damping property of the monolayer WS_2 plays an important role in explaining the sub- and super-radiant hybrid polariton states.

Figure 2(a) (left) gives the simulated reflectivity spectrum R (black curve) of the monolayer WS_2 covered on an unpatterned planar gold film with the incident angle $\theta = 15^\circ$. We can clearly see A exciton resonance at $\hbar\omega_X \approx 2.02$ eV, which is angle independent and consistent with the experimental result [37]. Note that the considerable decreasing slope in the reflectivity spectrum originates from the optical response of the gold film (red curve).

For the nanogroove array, we have chosen a narrow groove width of $w = 45$ nm and a shallow depth of $h_3 = 30$ nm to ensure narrow SPP resonances [31,44]. Such a nanogroove array, when illuminated with p-polarized light at incident angle θ, can support evanescent SPP fields excited at the air-metal (AM) interface by transferring momentum $n(2\pi/p)$ with $n \in \mathbf{Z}$, to the incident photons. To avoid interactions among different SPP modes, a small groove period $p = 430$ nm is properly chosen to only excite the AM[$n = -1$] SPP mode [14]. Figure 2(a) (right) presents the simulated reflectivity spectrum of the nanogroove array in absence of WS_2 overlayer, demonstrating the SPP excitation at $\hbar\omega_P = 2.05$ eV with the same incident angle. By varying the incident angle with $0^\circ \leqslant \theta \leqslant 30^\circ$, we can continuously shift the active SPP resonances between 2.1 and 1.8 eV, hence effectively tuning SPP into resonance with the WS_2 excitons. Figure 2(b) shows the 2D map of the simulated angle-resolved reflectivity spectra (in color scale). A typical anticrossing behavior (dashed arrows) indicates the strong X-SPP coupling and the formation of hybrid (energetically) upper (UP) and lower (LP) polariton modes. A normal mode splitting energy $\hbar\Omega_{NMS} = 2\hbar|\Omega_R| \approx 60$ meV can be identified from the prominent anticrossing of the UP and LP branch in the simulated reflectivity spectrum (solid black) at zero detuning $\delta = |\omega_X - \omega_P| = 0$ ($\theta = 15.4^\circ$),

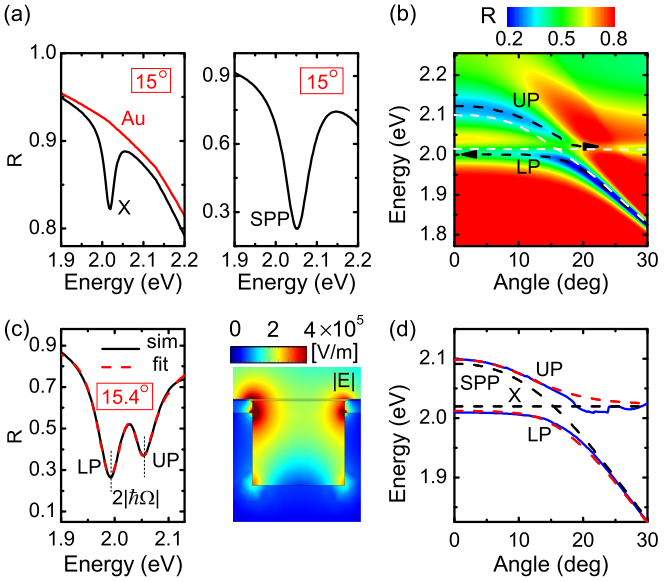

FIG. 2. (a) Simulated reflectivity spectra for an unpatterned planar gold-Al_2O_3 stack with (black) and without (red) monolayer WS_2 overlayer at an angle of incidence 15° (left), and the corresponding spectrum for a nanogroove array (right). (b) Simulated angle-dependent reflectivity spectra (in color scale) of the hybrid nanostructure overlapped with the coupled (dashed black arrows) and uncoupled (dashed white) mode dispersions. (c) Simulated and fitted reflectivity spectra of the hybrid system at $\theta = 15.4°$(left), and the corresponding electric field distribution at X resonance (right). (d) Dispersion relation of the coupled system obtained by a fitting (solid blue) and coupled oscillator model (dashed red).

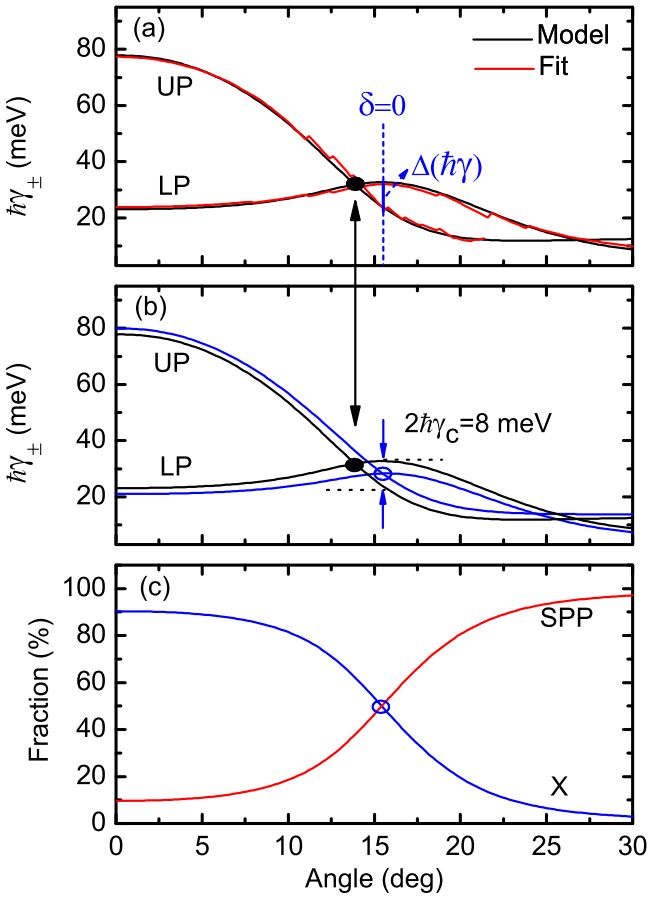

FIG. 3. (a) Polariton widths as a function of incident angle. The red and black solid lines indicate the result deduced from simulation and COM, respectively. (b) Polariton widths deduced from COM with (black solid line) and without (blue solid line) a cross damping term. (c) X and SPP fraction of the LP branch.

as shown in Fig. 2(c) (left). Here $\hbar|\Omega_R|$ denotes the X-SPP coupling strength. Figure 2(c) (right) illustrates the strong localization of the SPP electric fields $\vec{\mathbf{E}}$ for p-polarized excitation of 614 nm at $\theta = 15.4°$, corresponding to the X/SPP resonance. The calculations show strong evanescent SPP fields that are mainly localized near the groove region, revealing the fact that the strong coupling essentially results from the interaction of excitons and the localized SPP fields that are in close proximity to each other at the groove opening.

B. Coherent and incoherent X-SPP interactions

To give a deep insight into the X-SPP coupling property, we further extracted the optical characteristics of the hybrid UP and LP modes, including their dispersions and spectral widths, by fitting the simulated reflectivity spectra to a Fano-like line shape. The light reflected from our hybrid nanostructure comprises two different parts: nonresonant direct reflection from a gold interface and resonant excitation and subsequent re-emission of the polariton modes [16,31]. The interference between these two parts results in an asymmetric Fano-like line shape in the reflectivity spectra $R(\omega) = |r(\omega)|^2$ with

$$r(\omega) = a_b + \sum_{j=\mathrm{UP,LP}} \frac{b_j \gamma_j e^{i\phi_j}}{\omega - \omega_j + i\gamma_j}. \quad (2)$$

Here a_b is background amplitude. b_j and ϕ_j represent the amplitude and the spectral phase of the polariton modes, respectively. The spectral full width at half-maximum (FWHM) is characterized by $2\gamma_j$. We compare the fitted spectrum (dashed red) with the simulated result (solid black) in Fig. 2(c) for the angle of incidence $\theta = 15.4°$. The excellent match strongly suggests that a possible inhomogeneous broadening of the hybrid polariton modes does not exist (or negligible), thus showing only a minor contribution to their optical spectra.

From Eq. (2), the polariton energetics with a characteristic anticrossing feature can be accurately extracted, as presented in Fig. 2(d) by the solid blue lines. The deduced polariton widths $\hbar\gamma_\pm$, as shown in Fig. 3(a), exhibit an apparent angle-dependent decrease for the UP branch from ~80 down to ~10 meV and a slowly varying change around ~20 meV for the LP branch. Surprisingly, an apparent gap occurs around zero detuning. Particularly at zero detuning ($\delta = 0$), where the hybrid UP and LP modes are actually half-exciton-like and half-plasmon-like with equal X/SPP percentage of 50%, as demonstrated by the blue circle in Fig. 3(c), the UP width exceeds the LP width by $\Delta(\hbar\gamma) \approx 10$ meV. The considerable difference in UP and LP width might be taken as an indication that there exists an incoherent interaction process, which is induced by the coherent X-SPP coupling. This coupling-induced phenomena "open up" an additional incoherent damping pathway and

affect the radiative lifetimes, leading to sub/super-radiant (long/short-lived) hybrid states [17,47].

To reveal the underlying mechanism behind the interesting inequality of UP and LP width, we utilize the well-established coupled oscillator model (COM) [13,16,17], in which both the coherent and incoherent coupling processes can be quantitatively included in an effective non-Hermitian Hamiltonian. In the framework of COM, the individual excitonic and plasmonic system can be modeled as two coupled harmonic oscillators:

$$\hbar\left(\begin{bmatrix}\widetilde{\omega}_{\mathrm{X}} & \Omega_{\mathrm{R}}\\ \Omega_{\mathrm{R}}^{*} & \widetilde{\omega}_{\mathrm{P}}\end{bmatrix}-i\begin{bmatrix}0 & \gamma_{\mathrm{C}}\\ \gamma_{\mathrm{C}} & 0\end{bmatrix}\right)\begin{pmatrix}\alpha\\ \beta\end{pmatrix}=E\begin{pmatrix}\alpha\\ \beta\end{pmatrix}. \tag{3}$$

Here $\widetilde{\omega}_{\mathrm{X}}=\omega_{\mathrm{X}}-i\gamma_{\mathrm{X}}$ and $\widetilde{\omega}_{\mathrm{P}}=\omega_{\mathrm{P}}-i\gamma_{\mathrm{P}}$ represent the complex resonance frequencies of the uncoupled monolayer WS_2 excitons and SPPs, respectively. Their real parts give the eigenenergies of monolayer WS_2 exciton and SPP, which are depicted in Fig. 2(d) by black dashed lines. The imaginary parts represent population damping by radiative ($\Gamma_{j,\mathrm{rad}}$) and nonradiative ($\Gamma_{j,\mathrm{nonrad}}$) processes with damping rate $\Gamma_j=2\gamma_j=\Gamma_{j,\mathrm{rad}}+\Gamma_{j,\mathrm{nonrad}}$. Here the indices $j=\mathrm{X,P}$ denote the excitonic and plasmonic subsystem, respectively. An important cross-damping term γ_{C} is included to consider the influence of the incoherent interaction process [17,31]. We will show that the simulated optical characteristics of the hybrid system can be successfully reproduced provided that both coherent (Ω_{R}) and incoherent (γ_{C}) terms are taken into account. The absolute square of the eigenvectors $|\alpha|^2$ and $|\beta|^2$ give the weighting fractions of the individual excitonic and plasmonic system with $|\alpha|^2+|\beta|^2=1$. E denotes the eigenvalues corresponding to energetics of the hybrid polariton states.

In this model, the angle-independent excitonic energy and the total spectral width of WS_2 is taken as $\hbar\omega_{\mathrm{X}}=2.02$ eV and $\hbar\Gamma_{\mathrm{X,tot}}=28$ meV from the transmission spectra measured on substrate-supported high-quality exfoliated monolayer WS_2 at room temperature [37]. It is important to note that we consider the WS_2 excitonic linewidth to be homogeneously broadened with negligible inhomogeneous broadening, i.e., $\hbar\Gamma_{\mathrm{X,tot}}=\hbar\Gamma_{\mathrm{X}}+2\hbar\gamma_{\mathrm{X}}^{*}$ with γ_{X}^{*} representing pure dephasing processes. Spectroscopic measurements have revealed that the nonradiative decay dominates at room temperature, leading to a linewidth broadening $\hbar\Gamma_{\mathrm{X,\,nonrad}}$ over 20 meV. While the radiative damping gives a minor contribution to the linewidth of $\hbar\Gamma_{\mathrm{X,rad}}\approx 7$ meV [48]. This also implies that the broadening introduced by the pure dephasing processes can be neglected, that is $\gamma_{\mathrm{X}}^{*}=0$.

For the plasmonic system, the angle-dependent SPP dispersion $\hbar\omega_{\mathrm{P}}(\theta)$ and width $\hbar\Gamma_{\mathrm{P}}(\theta)=2\hbar\gamma_{\mathrm{P}}(\theta)$ are extracted from the simulated reflectivity spectra for a bare nanogroove in the absence of WS_2 overlayer. For such a shallow nanogroove array, our previous experimental work has shown that the SPP resonance width are in most cases dominated by the radiative broadening [16,17]. The nonradiative damping due to the Ohmic loss in metal and the pure dephasing process are negligible.

By solving Eq. (3) with optimized coupling energy $\hbar|\Omega_R|=32$ meV and the cross-damping term $\hbar\gamma_{\mathrm{C}}=-4$ meV, we can very nicely reproduce both the dispersion [dashed red lines in Fig. 2(d)] and polariton width [black lines in Fig. 3(a)] of the hybrid polariton modes, which are given by the real parts and the imaginary parts of the complex eigenvalues:

$$E_{\pm}=\hbar\widetilde{\omega}_{\pm}=\hbar\left(\frac{\widetilde{\omega}_{\mathrm{X}}+\widetilde{\omega}_{\mathrm{P}}}{2}\right)\pm\hbar\sqrt{\left(\frac{\widetilde{\omega}_{\mathrm{X}}-\widetilde{\omega}_{\mathrm{P}}}{2}\right)^{2}+\left(|\Omega_{\mathrm{R}}|^{2}-\gamma_{\mathrm{C}}^{2}\right)-2i\gamma_{\mathrm{C}}\mathrm{Re}(\Omega_{\mathrm{R}})}. \tag{4}$$

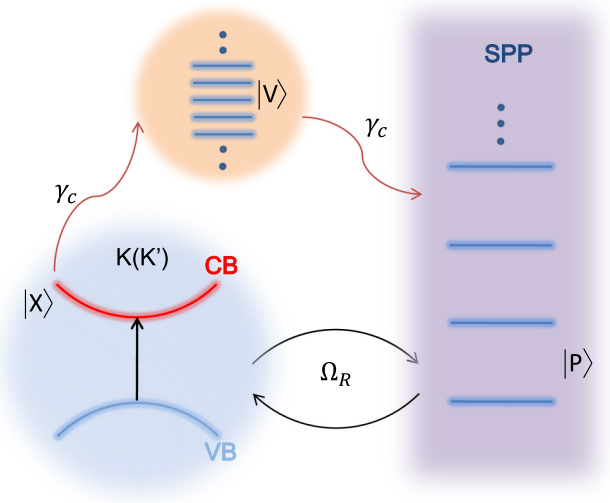

FIG. 4. Schematic of a strongly coupled exciton-SPP system. The excitonic system is modeled as a two-level system consisting of a conduction band (CB) and a valence band (VB). The plasmon system is represented as a photonic mode $|P\rangle$. The continuum of vacuum states is denoted as $|V\rangle$. The coherent energy transfer channel with coupling strength Ω_{R} is represented by the black arrows and the incoherent energy transfer channel through vacuum field with cross damping rate γ_{C} is denoted by the red arrows.

Particularly, the difference in the damping rates and the resulting inequality of the UP and LP width can be readily explained by Eq. (4). Apparently, in the strong coupling regime and at zero detuning with $\omega_{\mathrm{X}}=\omega_{\mathrm{P}}$, a difference in the UP and LP damping rates always exists for a nonzero γ_{C}, i.e., $\mathrm{Im}(\widetilde{\omega}_{+}-\widetilde{\omega}_{-})\neq 0$ holds since the last term under the root does not vanish. While in absence of the cross-damping term ($\gamma_{\mathrm{C}}=0$), the polariton widths, as shown by the blue lines in Fig. 3(b), exhibit a clear degeneracy with equal value of $\hbar(\Gamma_{\mathrm{X}}+\Gamma_{\mathrm{P}})/2$ at zero detuning (blue circle). This is because the damping rates of the polariton modes are linked to the mixing fraction ratios of excitonic and plasmonic parts, as shown in Fig. 3(c). On resonance (blue circle), the UP and LP states have identical decay rates with equal superposition of X and SPP wave functions.

Physically, we can understand the microscopic coupling process as follows: when the coupling strength exceeds the damping rates, i.e., $\Omega_{\mathrm{R}}>(\gamma_{\mathrm{X}}+\gamma_{\mathrm{P}})/2$, the system is in strong coupling regime [49,50]. As depicted in Fig. 4, the individual subsystem can strongly interact with each other via two types of coupling processes: (i) the coherent dipole-dipole interaction characterized by the Hermitian matrix element Ω_{R}, leading to a coherent exchange of energy (Rabi oscillations), and

importantly (ii) X and SPP can spontaneously emit photons into surrounding vacuum field modes and these photons can then be reabsorbed. This corresponds to an incoherent energy exchange process without conserving any phase relationship, which can be described by a coupling-induced damping term γ_C (red arrows). Generally, Ω_R and γ_C are not independent of each other but are related by a Kramers-Kronig relationship [47].

The coherent coupling strength $\hbar\Omega_R$ is generally determined by the exciton transition dipole moment μ_X, the number of exciton N_X involved in the coupling, and the strength of ambient confined vacuum SPP field E_{vac} [49]:

$$\hbar|\Omega_R| = \sqrt{N_X}\mu_X|E_{vac}|. \quad (5)$$

The dipole moment for the A exciton of WS_2 can be taken as $\mu_X \approx 50$ D [39], which is half of the value for J-aggregate excitons in our previously reported metal-molecular aggregate hybrid system [16,17]. Interestingly, the coherent coupling strength obtained here is also reduced by half with respect to $\hbar\Omega_R \approx 60$ meV in J-aggregate system [16]. Since the same gold nanogroove array is used for both cases with slightly different geometrical parameters, we assume a similar condition of vacuum field localization E_{vac} around the groove. Therefore, we can conclude from Eq. (5) that an ensemble of excitons with N_X on order of 2000, which is similar to the exciton number reported in Ref. [16], contribute to the coherent coupling process. Since the monolayer WS_2 is only atomic thick, much thinner than the 50-nm-thick spin-coated PVA film containing J-aggregates with an exciton density of $10^{24}/m^3$, it strongly indicates that the monolayer WS_2 possess much higher exciton density with uniform electronic and optical response over the entire 2D flake. This can remarkably benefit the strong coherent light-matter interactions with high integrability.

In contrast to the coherent coupling strength, the incoherent coupling strength is comparable to that for the J-aggregate case in our previous work [17]. However, the polariton modes exhibit distinctly different damping property for the two cases. In the J-aggregate system, we observed a pronounced anticrossing of angle-dependent polariton width with much broader UP width that exceeds LP width by over 20 meV at zero detuning [17]. This large width difference contains two contributions: (i) the dominating modification of polariton damping rates originated from the pure dephasing process in J-aggregate excitons, which scales linearly with the exciton weighting fractions, and (ii) the less prominent contribution from the formation of sub- and super-radiant polariton states due to the coupling-induced incoherent coupling process. While in the hybrid system considered in our study, we assume that pure dephasing do not exist in WS_2 excitons, the difference in polariton width is a direct consequence of the latter, corresponding to subradiant LP and super-radiant UP mode.

The coupling-induced cross damping term is directly linked to the damping rates and the orientation of the dipole moments of the subsystems, generally, $\gamma_C < \sqrt{\gamma_X\gamma_P}(\boldsymbol{\mu_X}\cdot\boldsymbol{\mu_P})$ holds [47]. The incoherent coupling strength can be further enhanced by having equal damping ($\gamma_X = \gamma_P$) and dipole moments aligned in parallel ($\boldsymbol{\mu_X} \parallel \boldsymbol{\mu_P}$), which results in the most efficient incoherent photon exchange and total dark/bright polariton states. In this sense, the present hybrid system provides an ideal platform for investigating strong interactions between TMD-based excitons and plasmonic excitations: even the monolayer of WS_2 is only atomically thick, it still can provide sufficiently strong coupling-induced incoherent damping with respect to that offered in our previous hybrid system where the J-aggregate film is over 50-nm thick [17]. This efficient incoherent interaction benefits from the highly confined WS_2 excitons in the in-plane direction so as to align the orientation of excitons with dipolar direction of SPPs for both coherent dipole-dipole interactions and effective coupling-induced incoherent interactions. The interplay between the X-SPP coherent dipole coupling and coupling-induced incoherent interactions not only determines the energetics of the hybrid system, but also governs the population damping properties of the polariton modes, thus providing an efficient approach to controlling of both coherent and incoherent polariton dynamics with flexible tunability. In principle, the sub- and super-radiant effects can be further verified by directly monitoring polariton population dynamics using time-resolved ultrafast pump-probe spectroscopy.

III. CONCLUSIONS

In summary, we have theoretically studied the interactions between two fundamentally distinct excitations, i.e., excitons in WS_2 and SPPs supported by a plasmonic nanogroove array in a strong coupling regime. A typical anticrossing behavior in the simulated static reflectivity spectra indicates a strong coherent X-SPP coupling with Rabi splitting of 60 meV. Importantly, we have demonstrated a considerable difference in polariton width, which is attributed to the formation of sub- and super-radiant polariton states due to an incoherent process of photon exchange between the two subsystems. By utilizing the coupled oscillator model and taking into account both a coherent interaction term and a coupling-induced cross damping term in a non-Hermitian matrix, we identify two interaction processes, i.e., coherent dipole-dipole interactions and coupling-induced incoherent exchange of photon energy in the strongly coupled hybrid system.

Our analysis strongly suggests that the optical properties of our hybrid system are largely governed by the interplay between the coherent X-SPP dipole coupling and the incoherent exchange of photon energy between both systems. Exploiting the highly tunable SPPs strongly coupled to TMD-based excitons controls not only the energetics of the systems but also the dynamics of the polariton modes. Particularly, the coupling leads to an efficient decoupling of the subradiant mode from the environment. Therefore, the spontaneous emission dynamics can be continuously controlled by adjusting their dipolar coupling and the damping property of the individual subsystems, thus providing a promising way of modifying the property of hybrid polariton states. This controllability, in combination with the flexible 2D "sheet" nature of monolayer TMDs offers a powerful approach for optimizing polariton dynamics. This is expected to be useful for realizing TMD-integrated active optoelectronic and plasmonic devices.

ACKNOWLEDGMENTS

This work was supported by the National Natural Science Foundation of China (Grants No. 61675139, No. 11474207) and the National Key R&D Program of China (2017YFA0303600).

[1] J. Kasprzak, M. Richard, S. Kundermann, A. Baas, P. Jeambrun, J. M. J. Keeling, F. M. Marchetti, M. H. Szymanska, R. Andre, J. L. Staehli, V. Savona, P. B. Littlewood, B. Deveaud, and L. S. Dang, Nature (London) **443**, 409 (2006).

[2] K. Hennessy, A. Badolato, M. Winger, D. Gerace, M. Atature, S. Gulde, S. Falt, E. L. Hu, and A. Imamoglu, Nature (London) **445**, 896 (2007).

[3] J. M. Raimond, M. Brune, and S. Haroche, Rev. Mod. Phys. **73**, 565 (2001).

[4] G. Khitrova, H. M. Gibbs, M. Kira, S. W. Koch, and A. Scherer, Nat. Phys. **2**, 81 (2006).

[5] S. Smolka, W. Wuester, F. Haupt, S. Faelt, W. Wegscheider, and A. Imamoglu, Science **346**, 332 (2014).

[6] P. Torma and W. L. Barnes, Rep. Prog. Phys. **78**, 013901 (2015).

[7] D. G. Baranov, M. Wersall, J. Cuadra, T. J. Antosiewicz, and T. Shegai, ACS Photon. **5**, 24 (2018).

[8] P. Vasa and C. Lienau, ACS Photon. **5**, 2 (2018).

[9] D. Martin-Cano, L. Martin-Moreno, F. J. Garcia-Vidal, and E. Moreno, Nano Lett. **10**, 3129 (2010).

[10] J. Bellessa, C. Bonnand, J. C. Plenet, and J. Mugnier, Phys. Rev. Lett. **93**, 036404 (2004).

[11] J. Dintinger, S. Klein, F. Bustos, W. L. Barnes, and T. W. Ebbesen, Phys. Rev. B **71**, 035424 (2005).

[12] Y. Sugawara, T. A. Kelf, J. J. Baumberg, M. E. Abdelsalam, and P. N. Bartlett, Phys. Rev. Lett. **97**, 266808 (2006).

[13] P. Vasa, R. Pomraenke, S. Schwieger, Y. I. Mazur, V. Kunets, P. Srinivasan, E. Johnson, J. E. Kihm, D. S. Kim, E. Runge, G. Salamo, and C. Lienau, Phys. Rev. Lett. **101**, 116801 (2008).

[14] P. Vasa, R. Pomraenke, G. Cirmi, E. De Re, W. Wang, S. Schwieger, D. Leipold, E. Runge, G. Cerullo, and C. Lienau, ACS Nano **4**, 7559 (2010).

[15] D. E. Gomez, K. C. Vernon, P. Mulvaney, and T. J. Davis, Nano Lett. **10**, 274 (2010).

[16] P. Vasa, W. Wang, R. Pomraenke, M. Lammers, M. Maiuri, C. Manzoni, G. Cerullo, and C. Lienau, Nat. Photon. **7**, 128 (2013).

[17] W. Wang, P. Vasa, R. Pomraenke, R. Vogelgesang, A. De Sio, E. Sommer, M. Maiuri, C. Manzoni, G. Cerullo, and C. Lienau, ACS Nano **8**, 1056 (2014).

[18] E. Elizner, K. Akulov, T. Schwartz, and T. Ellenbogen, Nano Lett. **17**, 7675 (2017).

[19] S. A. Maier, P. G. Kik, H. A. Atwater, S. Meltzer, E. Harel, B. E. Koel, and A. A. G. Requicha, Nat. Mater. **2**, 229 (2003).

[20] S. I. Bozhevolnyi, V. S. Volkov, E. Devaux, J. Y. Laluet, and T. W. Ebbesen, Nature (London) **440**, 508 (2006).

[21] S. Lal, S. Link, and N. J. Halas, Nat. Photon. **1**, 641 (2007).

[22] N. T. Fofang, T.-H. Park, O. Neumann, N. A. Mirin, P. Nordlander, and N. J. Halas, Nano Lett. **8**, 3481 (2008).

[23] T. K. Hakala, J. J. Toppari, A. Kuzyk, M. Pettersson, H. Tikkanen, H. Kunttu, and P. Torma, Phys. Rev. Lett. **103**, 053602 (2009).

[24] T. Schwartz, J. A. Hutchison, C. Genet, and T. W. Ebbesen, Phys. Rev. Lett. **106**, 196405 (2011).

[25] S. A. Guebrou, C. Symonds, E. Homeyer, J. C. Plenet, Y. N. Gartstein, V. M. Agranovich, and J. Bellessa, Phys. Rev. Lett. **108**, 066401 (2012).

[26] R. H. Dicke, Phys. Rev. **93**, 99 (1954).

[27] R. G. DeVoe and R. G. Brewer, Phys. Rev. Lett. **76**, 2049 (1996).

[28] S. H. Lim, T. G. Bjorklund, F. C. Spano, and C. J. Bardeen, Phys. Rev. Lett. **92**, 107402 (2004).

[29] Y. N. Chen, D. S. Chuu, and T. Brandes, Phys. Rev. Lett. **90**, 166802 (2003).

[30] M. Hubner, J. Kuhl, T. Stroucken, A. Knorr, S. W. Koch, R. Hey, and K. Ploog, Phys. Rev. Lett. **76**, 4199 (1996).

[31] C. Ropers, D. J. Park, G. Stibenz, G. Steinmeyer, J. Kim, D. S. Kim, and C. Lienau, Phys. Rev. Lett. **94**, 113901 (2005).

[32] H. Wang, D. W. Brandl, F. Le, P. Nordlander, and N. J. Halas, Nano Lett. **6**, 827 (2006).

[33] Y. Sonnefraud, N. Verellen, H. Sobhani, G. A. E. Vandenbosch, V. V. Moshchalkov, P. Van Dorpe, P. Nordlander, and S. A. Maier, ACS Nano **4**, 1664 (2010).

[34] B. Luk'yanchuk, N. I. Zheludev, S. A. Maier, N. J. Halas, P. Nordlander, H. Giessen, and C. T. Chong, Nat. Mater. **9**, 707 (2010).

[35] A. Chernikov, T. C. Berkelbach, H. M. Hill, A. Rigosi, Y. Li, O. B. Aslan, D. R. Reichman, M. S. Hybertsen, and T. F. Heinz, Phys. Rev. Lett. **113**, 076802 (2014).

[36] J. Cuadra, D. G. Baranov, M. Wersall, R. Verre, T. J. Antosiewicz, and T. Shegai, Nano Lett. **18**, 1777 (2018).

[37] S. Wang, S. Li, T. Chervy, A. Shalabney, S. Azzini, E. Orgiu, J. A. Hutchison, C. Genet, P. Samori, and T. W. Ebbesen, Nano Lett. **16**, 4368 (2016).

[38] J. Wen, H. Wang, W. Wang, Z. Deng, C. Zhuang, Y. Zhang, F. Liu, J. She, J. Chen, H. Chen, S. Deng, and N. Xu, Nano Lett. **17**, 4689 (2017).

[39] D. Zheng, S. Zhang, Q. Deng, M. Kang, P. Nordlander, and H. Xu, Nano Lett. **17**, 3809 (2017).

[40] W. J. Liu, B. Lee, C. H. Naylor, H. S. Ee, J. Park, A. T. C. Johnson, and R. Agarwal, Nano Lett. **16**, 1262 (2016).

[41] X. Z. Liu, T. Galfsky, Z. Sun, F. N. Xia, E. C. Lin, Y. H. Lee, S. Kena-Cohen, and V. M. Menon, Nat. Photon. **9**, 30 (2015).

[42] S. Dufferwiel, S. Schwarz, F. Withers, A. A. P. Trichet, F. Li, M. Sich, O. Del Pozo-Zamudio, C. Clark, A. Nalitov, D. D. Solnyshkov, G. Malpuech, K. S. Novoselov, J. M. Smith, M. S. Skolnick, D. N. Krizhanovskii, and A. I. Tartakovskii, Nat. Commun. **6**, 8579 (2015).

[43] M. Sidler, P. Back, O. Cotlet, A. Srivastava, T. Fink, M. Kroner, E. Demler, and A. Imamoglu, Nat. Phys. **13**, 255 (2017).

[44] D. S. Kim, S. C. Hohng, V. Malyarchuk, Y. C. Yoon, Y. H. Ahn, K. J. Yee, J. W. Park, J. Kim, Q. H. Park, and C. Lienau, Phys. Rev. Lett. **91**, 143901 (2003).

[45] Y. Li, A. Chernikov, X. Zhang, A. Rigosi, H. M. Hill, A. M. van der Zande, D. A. Chenet, E.-M. Shih, J. Hone, and T. F. Heinz, Phys. Rev. B **90**, 205422 (2014).

[46] A. Shalabney, J. George, J. Hutchison, G. Pupillo, C. Genet, and T. W. Ebbesen, Nat. Commun. **6**, 5981 (2015).

[47] U. Akram, Z. Ficek, and S. Swain, Phys. Rev. A **62**, 013413 (2000).

[48] M. Selig, G. Berghaeuser, A. Raja, P. Nagler, C. Schueller, T. F. Heinz, T. Korn, A. Chernikov, E. Malic, and A. Knorr, Nat. Commun. **7**, 13279 (2016).

[49] R. J. Thompson, G. Rempe, and H. J. Kimble, Phys. Rev. Lett. **68**, 1132 (1992).

[50] G. Rempe, R. J. Thompson, and H. J. Kimble, Phys. Scripta **T51**, 67 (1994).